J Inorg Organomet Polym (2013) 23:306–314
DOI 10.1007/s10904-012-9776-7

Negative Permittivity of Polyaniline–Fe_3O_4 Nanocomposite

H. Kavas · M. Günay · A. Baykal · M. S. Toprak · H. Sozeri · B. Aktaş

Received: 27 August 2012 / Accepted: 3 October 2012 / Published online: 16 October 2012

Abstract Polyaniline–Fe_3O_4 nanocomposite with and without ionic liquid were successfully synthesized via in situ polymerization using cetyl trimethylammonium bromide (CTAB) as surfactant. Both TG analysis and FT-IR measurements proved the presence of organic layer on the surface of Fe_3O_4 nanoparticles. The influence of 1-butyl-3-methyl-imidazolium bromide (BMIMBr) as ionic liquid on the structure, conductivity, and magnetic property of PANI–Fe_3O_4–CTAB nanocomposite were studied in detail. The results show that imidazolium-based ionic liquids BMIMBr acts as an anchor agent during the formation of PANI–Fe_3O_4–CTAB nanocomposite. Ionic liquid significantly deteriorated nanocomposite's magnetic properties, and contributed to non-saturated M–H curve due to the disappearance of antiferromagnetic interactions. It has also an improving effect on AC and DC conductivities. The most important effect of IL is observed in real part of permittivity of PANI–Fe_3O_4–CTAB that it has negative high values at low frequency low temperature region. Due to the negative dielectric constant, material exhibits uncommon properties in electromagnetic waves scattering and attraction between similar charges. This possibility provokes research on these composites as high T superconductors, negative index materials and microwave absorbers.

Keywords Magnetic nanomaterials · Electrical properties · Magnetic properties · Negative permittivity · Ionic liquid

H. Kavas (✉) · B. Aktaş
Physics Department, Gebze Institute of Technology (GYTE), 41400 Gebze, Kocaeli, Turkey
e-mail: hkavas@gyte.edu.tr; hkavas@medeniyet.edu.tr

H. Kavas
Department of Engineering Physics, Istanbul Medeniyet University, Istanbul 34720, Turkey

M. Günay · A. Baykal (✉)
Department of Chemistry, Fatih University, 34500 Büyükçekmece, Istanbul, Turkey
e-mail: hbaykal@fatih.edu.tr

M. S. Toprak
Functional Materials Division, KTH Royal Institute of Technology, 16440 Stockholm, Sweden

M. S. Toprak
Department of Materials Science and Engineering, Yildirim Beyazit University, Ulus, Ankara, Turkey

H. Sozeri
TUBITAK-UME, National Metrology Institute, P.O. Box 54, 41470 Gebze, Kocaeli, Turkey

1 Introduction

Core–shell nanocomposites (metal oxide core which is covered by a conducting polymer shell) of inorganic and organic material are of special interest due to the combination of several very different properties. The inorganic compound, in this case iron oxide, provides magnetic properties and the organic compound, the conducting polymer, provides tuneable electronic conductivity [1]. Possible applications of this type of nanocomposites are electromagnetic shielding, electro-chemical display devices and microwave-absorbing material.

Magnetic polymer nanocomposites are a result of the combination of polymers and inorganic fillers at the nanometer scale. Organic–inorganic nanocomposites have received greater attention over the last decade because of the interesting possibilities for their structural modifications and promising potential applications in chemistry, biology,

medicine, and material science. A wide range of organic and inorganic materials can be combined to form nanocomposites with unique electrical, catalytic, and optical properties [2]. Among the existing conducting polymers (polyaniline (PANI), polypyrrole (PPy) and polythiophene (PTh)), PANI gets special attention due to its good environmental stability, easy doping or dedoping by chemical means and facile synthesis as it can be readily prepared in bulk by chemical oxidative polymerization of aniline under controlled conditions and it shows sufficient stability for practical applications [3]. PANI usually combined with other inorganic components to form nanocomposites in order to improve physical, mechanical, and electrical properties such as enhanced solubility, conductivity, magnetic, and optoelectronic properties, etc. [4]. Magnetic–conductive composites with an organized structure usually provide a new functional hybrid, which has synergetic or complementary behavior between magnetic and conductive materials [4].

Room-temperature ionic liquids (RTILs), a set of environmentally solvents with a relatively wide electrochemically stable window, good electrical conductivity, high ionic mobility, a broad range of room temperature liquid compositions, etc., have attracted increasing interest [5]. In particular, imidazolium ionic liquids associated with specific anions are known to self-organize in away that is adaptable to the fabrication of nanostructures of conducting polymers and inorganic materials [5]. In general, the preparation of organic–inorganic composites often results in pollution.

Zhu and co-workers [6] demonstrated that CTAB was a useful surfactant to be used for preventing Fe_3O_4 nanoparticles from agglomeration, and it has been found out that CTAB also played a very important role for the coating of Fe_3O_4 nanoparticles by PANI. The study showed that CTAB could produce insoluble substance with initiator of polyreaction, and play a very important role for the formation of PANI/Fe_3O_4 nanocomposites.

In the present work, we describe a facile and eco-friendly method of synthesizing PANI–Fe_3O_4–CTAB and PANI–Fe_3O_4–CTAB–IL nanocomposites at the interface of water and ionic liquid, respectively. The influence of imidazolium based ionic liquids on the morphology, structure, conductivity, and magnetic properties of PANI–Fe_3O_4–CTAB nanocomposite were investigated in detail. To the best of our knowledge, there is no report on the conducting PANI–Fe_3O_4–CTAB nanocomposites prepared with ionic liquids until now.

2 Experimental

2.1 Chemicals

Iron (III) chloride hexahydrate, $FeCl_3{\cdot}6H_2O$, and Iron (II) chloride tetrahydrate, $FeCl_2{\cdot}4H_2O$, aniline monomer, cetyl trimethylammonium bromide (CTAB) and sodium hydroxide (NaOH) were all obtained from Merck and 1-butyl-3-methyl-imidazolium bromide (BMIMBr) from Alfa–Aesar. They were used as-received, without further purification.

2.2 Instrumentation

X-ray powder diffraction (XRD) analysis was conducted on a Rigaku Smart Lab operated at 40 kV and 35 mA using Cu Kα radiation ($\lambda = 1.54059$ Å).

Fourier transform infrared (FT-IR) spectra of the samples were recorded with a Perkin Elmer BX FT-IR infrared spectrometer in the range of 4,000–400 cm^{-1}.

VSM measurements were performed by using a Vibrating sample magnetometer (LDJ Electronics Inc., Model 9600) and magnetization measurements were carried out in an external field up to 15 kOe at room temperature.

Transmission electron microscopy (TEM) analysis was performed using a FEI Tecnai G2 Sphera microscope. A drop of diluted sample in alcohol was dripped on a TEM grid.

The electrical conductivity of the PANI–Fe_3O_4–CTAB and PANI–Fe_3O_4–CTAB–IL nanocomposites was studied in the temperature range of 20–120 °C with a heating rate of 10 °C min^{-1}. The sample was used in the form of circular pellets of 13 mm diameter and 3 mm thickness. The pellets (both nanocomposite and pristine) were sandwiched between gold electrodes and the conductivities were measured using Novo-control dielectric impedance analyzer in the frequency range 1 Hz–3 MHz, respectively. The temperature (between −100 and 250 °C) was controlled with a Novo-cool Cryosystem.

The thermal stabilities of nanocomposites were determined by thermo gravimetric analysis (TGA, Perkin Elmer Instruments model, STA 6000). The TGA thermograms were recorded for 5 mg of powder sample at a heating rate of 10 °C min^{-1} in the temperature range of 30–750 °C under nitrogen atmosphere.

2.3 Procedure

Fe_3O_4 NP's were prepared by a hydrothermal method using CTAB as the surfactant. To 80 mL aqueous solutions containing 0.01 mol $FeCl_2{\cdot}4H_2O$, 0.02 mol $FeCl_3{\cdot}6H_2O$, and 0.7 g CTAB, 2 M NaOH was added drop by drop till pH reached 10.5 under vigorous stirring at 90 °C for 1 h under Ar gas. The obtained suspension was transferred into 50 mL stainless steel autoclave, after sealing the autoclave was put into an oven heated at 160 °C for 12 h and then cooled naturally to room temperature. Finally, the product was washed with distilled water and ethanol several times

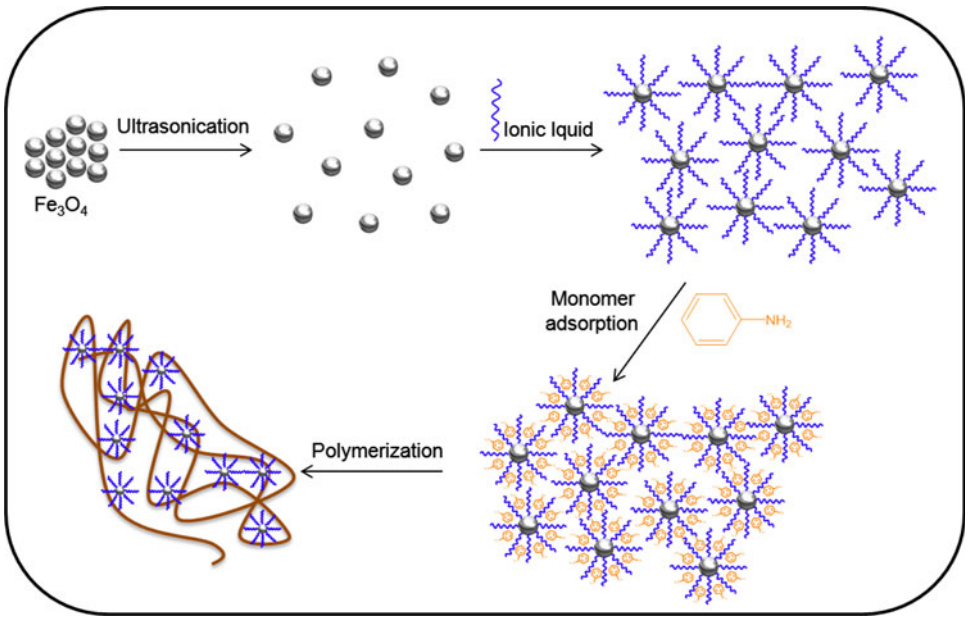

Scheme 1 Scheme of the fabrication of PANI-Fe_3O_4-CTAB-IL nanocomposite

to remove the impurities and dried in an oven at 100 °C for 2 h. 1 g as-prepared Fe_3O_4 NP's and 5.0 mL BMIMBr, IL were dispersed in dilute HCl solution (10^{-6} M) in a three-neck round-bottom flask fitted with ultrasonic vibration for 1 h, then 1.8 mL aniline monomer was added to the above mixture, and ultrasonic vibration was continued for another 30 min. The reaction system was then cooled in an ice bath. Under the protection with nitrogen gas, the ammonium peroxydisulfate (5 g, dissolved in 1.8 M HCl solution), which serves as an oxidant, was added drop-wise into this mixture. The reaction was continued for 18 h at 0 °C (Scheme 1). During sonication, the surfactant is adsorbed and arranged regularly at the Fe_3O_4 surfaces to inhibit Fe_3O_4 nanoparticles from agglomeration. The resulting nanocomposties are then stabilized by the regenerative surfactant CTAB. The same synthesis procedure was also used for the synthesis of PANI–Fe_3O_4–CTAB nanocomposite without IL. In this case, only IL was not used, and the rest of the process was the same with the synthesis of PANI–Fe_3O_4–CTAB–IL. Overall process is shown in Scheme 1.

3 Results and Discussion

3.1 XRD Analysis

The XRD patterns PANI–Fe_3O_4–CTAB nanocomposite and PANI–Fe_3O_4–CTAB–IL nanocomposite are shown in Fig. 1a, b, respectively. The main characteristic peaks were identified as cubic spinel structure of Fe_3O_4 [7–9]. These characteristic peaks of Fe_3O_4 nanoparticles can all be observed in the XRD patterns of the PANI–Fe_3O_4–CTAB and PANI–Fe_3O_4–CTAB–IL nanocomposites. So, the existence of Fe_3O_4 in both nanocomposites was thus confirmed.

All of the observed diffraction peaks are indexed by the cubic structure of Fe_3O_4 (JCPDS no. 19-629) revealing a high phase purity of magnetite. The XRD pattern of PANI–Fe_3O_4–CTAB (Fig. 1a) shows that PANI has partly crystalline structure and the two broad peaks are observed at $2\theta = 20.41$ and 25.61° [10, 11]. Both samples have an amorphous contribution to the background, however, the sharpness of XRD peaks reveal crystallinity of the nanoparticles. The mean size of the crystallites was estimated from the diffraction pattern by line profile fitting method using the Eq. (1) given [12, 13]. The line profile, shown in Fig. 1 was fitted for observed six peaks with the following miller indices: (220), (311), (400), (422), (511), and (440). The average crystallite size, D, was obtained as 10.0 ± 0.1 nm as a result of this line profile fitting.

3.2 FT-IR Analysis

FT-IR spectra of IL, CTAB, PANI–Fe_3O_4–CTAB nanocomposites with and without IL are presented in Fig. 2. The peaks (in Fig. 2c, d) at 583 cm^{-1} can be attributed to Fe–O bond [14–17] in PANI–Fe_3O_4–CTAB and PANI–Fe_3O_4–CTAB–IL nanocomposites. For PANI–Fe_3O_4–CTAB–IL nanocomposite, the bands at 1,630 and 3,410 cm^{-1} can be assigned to the O–H stretching vibrations; the bands at 1,568 and 1,472 cm^{-1} are attributed to the C=N and C=C stretching modes for the quinonoid and benzenoid units (N=Q=N [Q refers to the quinonic-type rings]), respectively; the bands at 1,290 and 1,247 cm^{-1} are attributed to C–N stretching mode for the benzenoid

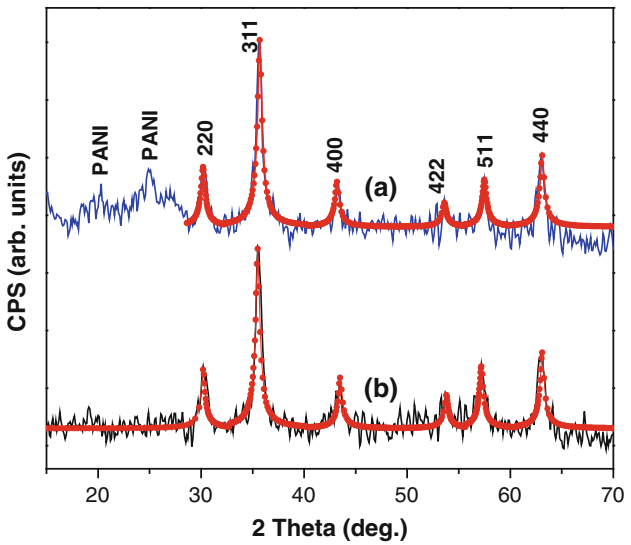

Fig. 1 XRD pattern of PANI–Fe_3O_4–CTAB nanocomposite *a* without IL, *b* with IL

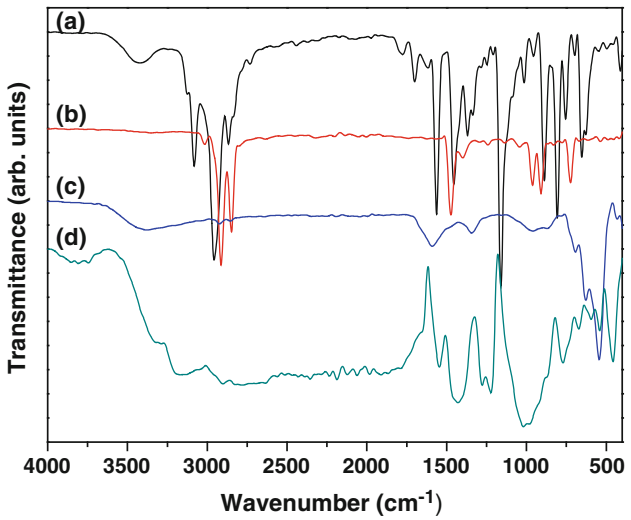

Fig. 2 FT-IR spectra of *a* CTAB, *b* IL, PANI–Fe_3O_4–CTAB nanocomposite, *c* without IL, and *d* with IL

unit; and the band at 1,110 cm^{-1} is assigned to an in-plane bending vibration of C–H which was formed during protonation [18–21]. For vibrations above 3,000 cm^{-1} peaks can be seen arising from imidazolium ring at 3,170 cm^{-1} (ring H–C–C–H asymmetric stretch) and 3,126 cm^{-1} (N=C stretch) [22–25]. The adsorption of IL onto PANI–Fe_3O_4–CTAB nanocomposite was evident from the appearance of the characteristic absorption peak of IL at the spectrum of the PANI–Fe_3O_4–CTAB–IL nanocomposite.

3.3 TG Analysis

Thermal stability of as-made for PANI–Fe_3O_4–CTAB nanocomposite with and without IL was analyzed by

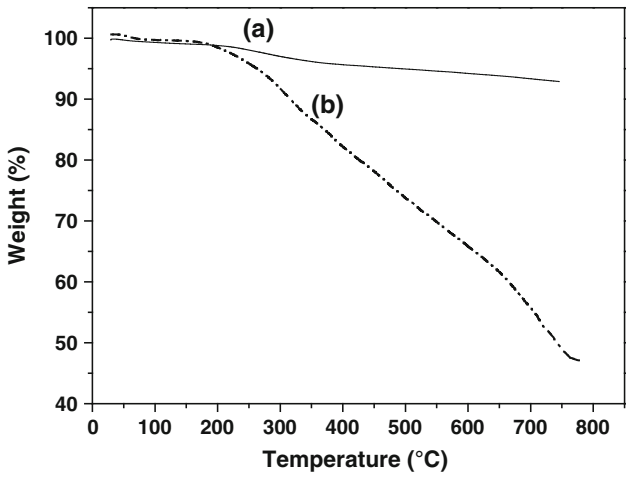

Fig. 3 TGA thermograms of *a* PANI–Fe_3O_4–CTAB nanocomposite and *b* PANI–Fe_3O_4–CTAB–IL nanocomposite

thermal gravimetric analysis and the resultant thermograms were presented in Fig. 3. An overall weight loss of ~55 and 10 % were observed for the PANI–Fe_3O_4–CTAB nanocomposite with and without IL, respectively. In case of the nanocomposite with IL, 5 % loss up to 200 °C is attributed to adsorbed water and the rest 50 % to decomposition of organic residues of IL, PANI, and CTAB. In the case of the nanocomposite without IL, ~3 % loss is due to adsorbed and crystalline water (up to 200 °C) and ~7 % organic PANI–CTAB components that totally decompose stabilizing the weight at 900 °C. TGA analysis indicate that nanocomposite with IL contains only 45 % inorganic ferrite phase while the that without IL contains 90 % inorganic ferrite phase, the rest being the organic components [26].

3.4 TEM Analysis

Morphology of nanoparticles has been investigated by TEM and few micrographs taken at various magnifications are presented in Fig. 4. Fe_3O_4 nanoparticles were observed to have a mixture of near spherical and polygonic morphology with particles having sizes in the range of 5 and 20 nm. Nanoparticles are well separated by the polymer intercalation, which is also visible in the micrographs, which in turn will affect the magnetic interaction between the nanoparticles.

3.5 VSM Measurements

The room temperature magnetization hysteresis of nanocomposites in the range of −15,000 to 15,000 Oe magnetic field is shown in Fig. 5. Since each of the magnetite nanoparticles can be treated as a thermally agitated permanent magnet in the carrier medium, magnetite and most

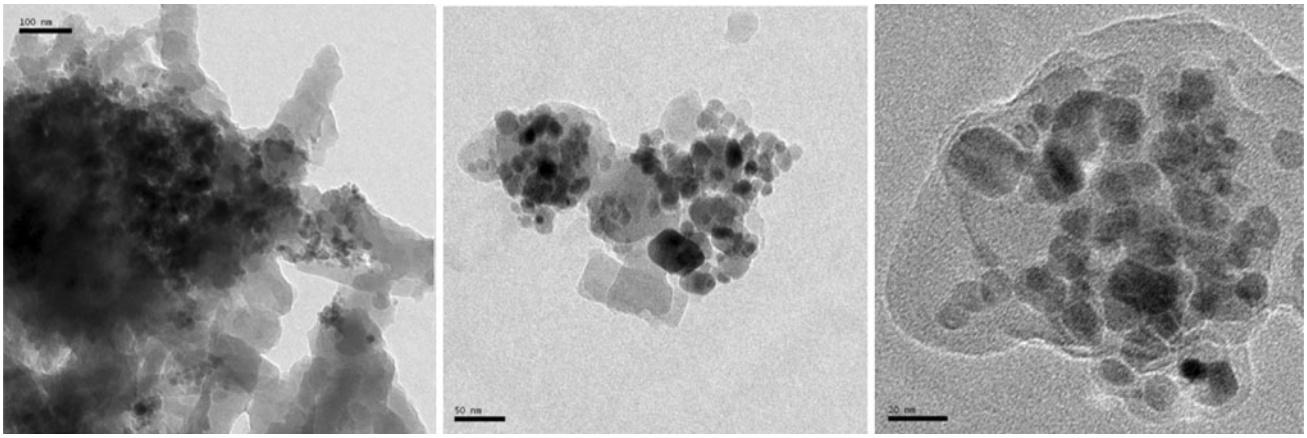

Fig. 4 TEM micrographs of PANI–Fe_3O_4–CTAB–IL nanocomposite at various magnifications

of its composites usually show a superparamagnetic behavior at room temperature. The applied magnetic field forces to align magnetic moments of the particles, then all these moment are leading to a macroscopic magnetization of the sample with field. The magnetization of these giant magnetic moments with field is in paramagnetic nature. The superparamagnetic magnetization of samples with non-hysteric magnetization loops (M–H curves) can explained by particle size. At smaller sizes, the magnetic moment of the particle as a whole is free to fluctuate in response to thermal energy, while the individual atomic moments maintain their ordered state relative to each other. The obtained saturation magnetization (M_s) at room temperature were 10.9, 52, and 64 emu g^{-1} for PANI–Fe_3O_4–CTAB–IL nanocomposite (Fig. 5), PANI–Fe_3O_4–CTAB nanocomposite (Fig. 5 inset a) and bulk Fe_3O_4 NP (Fig. 5 inset b), respectively. While they are similar in means of no coercive field (H_c), the saturation magnetization behaviors are changing. The bulk Fe_3O_4 NP and PANI–Fe_3O_4–CTAB nanocomposite don't reach saturation although the high applied magnetic field of 1.5 T. However, the sample PANI–Fe_3O_4–CTAB with IL has saturated magnetic characteristic at elevated temperatures. The reported M_s value of bulk Fe_3O_4 is between 92 and 97 emu g^{-1} [27] so the lower M_s values obtained here can be attributed to the presence of non-magnetic (dead) surface layer or compositional variations, superparamagnetic relaxation and spin canting because of antiferromagnetic interactions among the Fe spins in the nanomaterial [28]. The drastic decrease in M_s for sample PANI–Fe_3O_4–CTAB–IL may be caused by surface treatment of Fe_3O_4 NP by IL. The surface of magnetic NPs has weak combined action of interfacial (Van der Waals or acid–base) and magnetic attractions between the particles. Additionally the static repulsion produced by IL between particles inhibits them from agglomeration [29]. While the antiferromagnetic effect seen at higher fields with non saturation trend for the Fe_3O_4 NP and PANI–Fe_3O_4–CTAB samples, the sample of PANI–Fe_3O_4–CTAB–IL has just ferromagnetic interacting nature with saturated curve.

3.6 Electrical Properties

The conductivity and the dielectric constant of composites were measured between two electrodes at different temperature ranging from 20 to 120 °C in frequency range of 1 Hz–3 MHz. The AC conductivities, σ_{AC}, of samples are shown in Fig. 6. While the Sample PANI–Fe_3O_4–CTAB has σ_{AC} with wavy characteristic, the nanocomposite sample with IL has conductivity curves as a combination of steady part up to 10^5 Hz with an exponentially increasing part above this frequency. At high frequencies both samples show conductivity at the order of 10^{-4}–10^{-6}, however, at lower frequencies the conductivity curves drop sharply to the lower conduction values for nanocomposite sample without IL. In all frequency ranges, the σ_{AC} has higher values at increasing temperature for the sample without IL, but σ_{AC} has higher values at around 70 °C then it drops to lower values.

The DC conductivities were obtained by the extrapolation of AC curves to the zero frequency and are shown in Fig. 7. These curves were theoretically fitted by equation of $\ln(\sigma) = \ln(\sigma_o) - \frac{E_A}{kT}$ for both samples, where E_A is the activation energy. E_A were obtained as 0.136 eV and 0.147 eV for PANI–Fe_3O_4–CTAB and PANI–Fe_3O_4–CTAB–IL, respectively. The IL form of compound causes the increase in activation energies. In our previous works, E_A were found and reported as 0.050 and 0.044 eV for L-lysine coated iron oxide composites [30], 0.630 and 0.247 eV for PVTri–Fe_3O_4 nanocomposite systems [31], 0.674 and 0.110 eV for salicylic acid–Fe_3O_4 [32], 0.312 eV for L-histidine coated iron oxide NPs [7], 0.251 and 0.265 eV for carnosine coated Fe_3O_4 [16], 0.293 and 4.231 eV for PPPA/Fe_3O_4–NPs [33]. The variation of EA

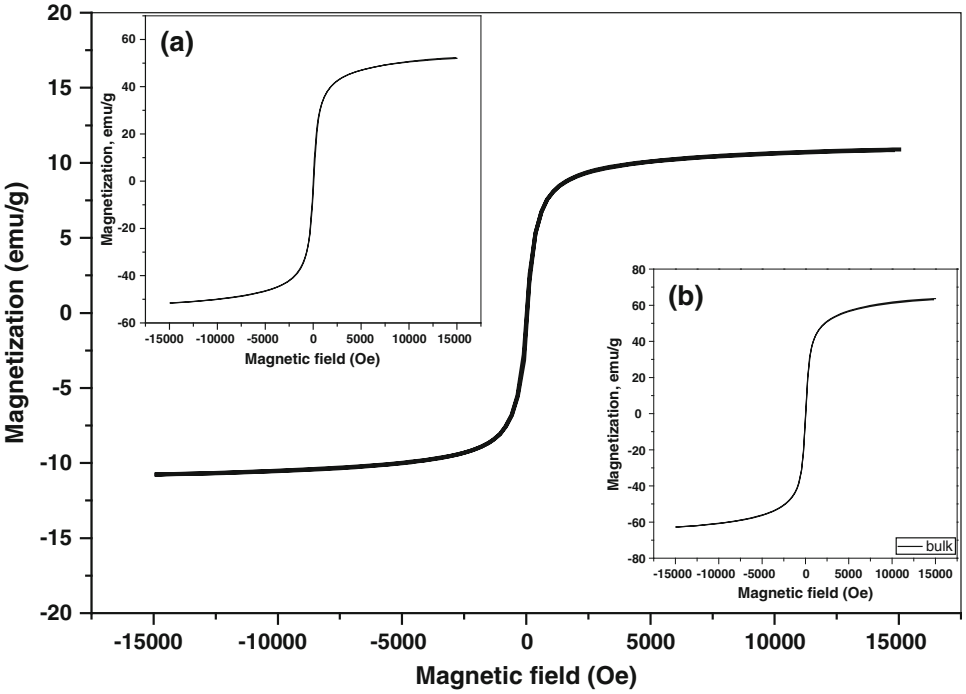

Fig. 5 Room temperature magnetization curve for PANI–Fe_3O_4–CTAB–IL; in the *inset* *a* PANI–Fe_3O_4–CTAB nanocomposite; and *b* bulk Fe_3O_4 NP

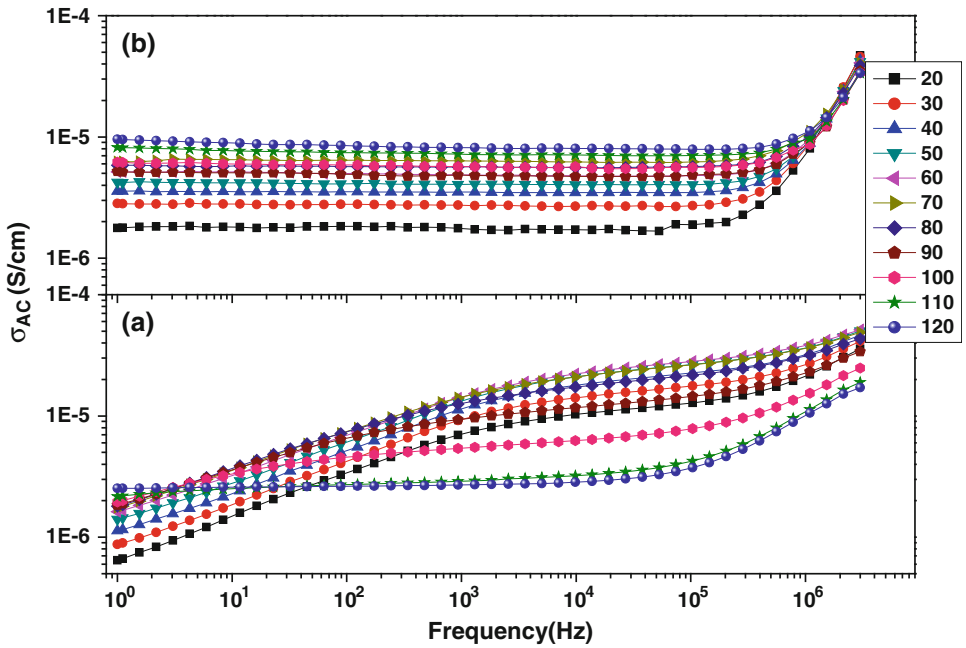

Fig. 6 AC conductivity as a function of log (frequency) for PANI–Fe_3O_4–CTAB sample with (*a*) and without (*b*) IL, at different temperatures

may be caused by various polymeric media coated on Fe_3O_4 and different conduction mechanism for nanocomposites prepared via different routes. The likely hydrogen bonding between the hydroxyl groups on the surface of magnetite and –N= in the PANI molecular chains create an intermediate layer with more insulating role and so it may cause the slight increase of E_A in composite with IL. The AC conductivity of composites versus angular frequency ($\omega = 2\ \pi$ f) curves were fitted with respect to AC power law ($\sigma = B\omega^n$) and n is found to decrease with increasing temperature (not shown here). As a result the effective conduction mechanism is found as correlated barrier hopping (CBH) the nature of n (T) [16].

The real part of permittivity as a function of frequency at various temperatures is illustrated for both samples in Fig. 8. There is a significant difference between the ε' of the samples such that PANI–Fe_3O_4–CTAB has positive values of ε' while PANI–Fe_3O_4–CTAB–IL exhibit negative values of ε'. IL may have changed the dielectric nature of the nanocomposite sample. The large resonance at low

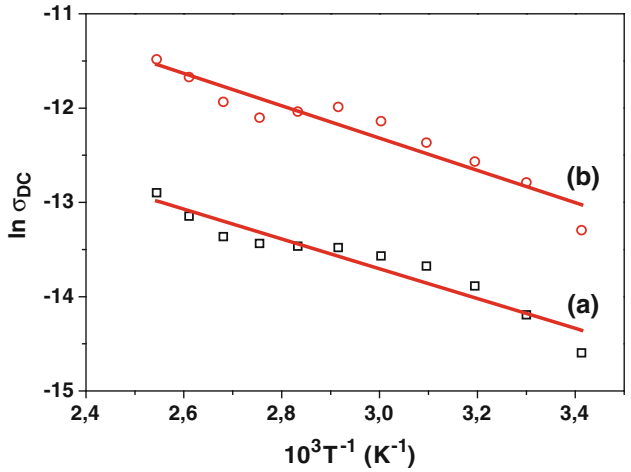

Fig. 7 The Arrhenius plot $(\ln(\sigma)\, vs.\, 1,000/T)$ and fits of DC conductivity curves of *a* PANI–Fe_3O_4–CTAB and *b* PANI–Fe_3O_4–CTAB–IL as a function of frequency at various temperatures

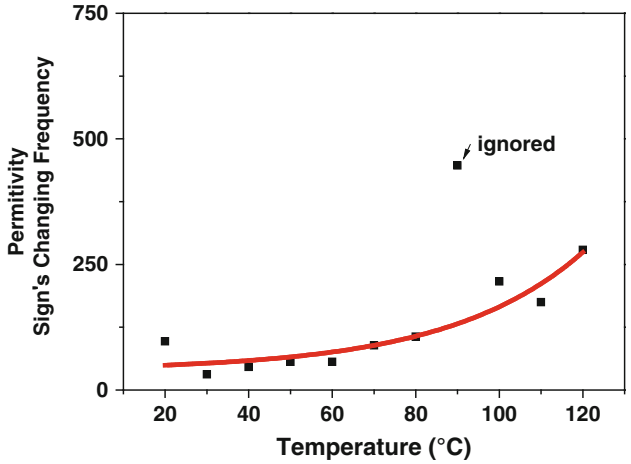

Fig. 9 Permittivity sign changing frequency with respect to temperature for sample PANI–Fe_3O_4–CTAB–IL

frequencies may lead such variation in dielectric nature of system. The composite with IL has an intermediate bounding between magnetite and the PANI which may have resonance at such low frequencies. The induction of polarization at high frequencies is causing the switching permittivity from negative to positive.

The ε' of PANI–Fe_3O_4–CTAB–IL sample has exponentially decaying curves with increasing frequency and by increasing temperature. Such nanocomposite preparation with IL gives a negative dielectric permittivity with ε' about same magnitude. The ε' of PANI–Fe_3O_4–CTAB–IL generally has positive values as sample without IL but at lower frequencies it suddenly changes sign to negative and reach higher negative values. While ε' curves decrease when frequency goes to DC character for high temperature, the ε' curves for lower temperatures has fluctuating characteristic between + and − sign at lower frequencies. They again turn positive values of ε' but never reach their maximum values with negative sign. Such PANI composites with negative permittivity were reported for polymeric composites of PANI–DBSA (dodecylbenzene sulfonic acid)/polyacrylic acid (PAA) with low PANI content of 2 and 4 % [34]. Other studies based on PANI composites with negative permittivity were also reported for camphor sulfonic acid (CSA)/PANI sample [35–37] for urea-coated

Fig. 8 Real part of permittivity of samples *a* PANI–Fe_3O_4–CTAB and *b* PANI–Fe_3O_4–CTAB–IL as a function of frequency at various temperatures

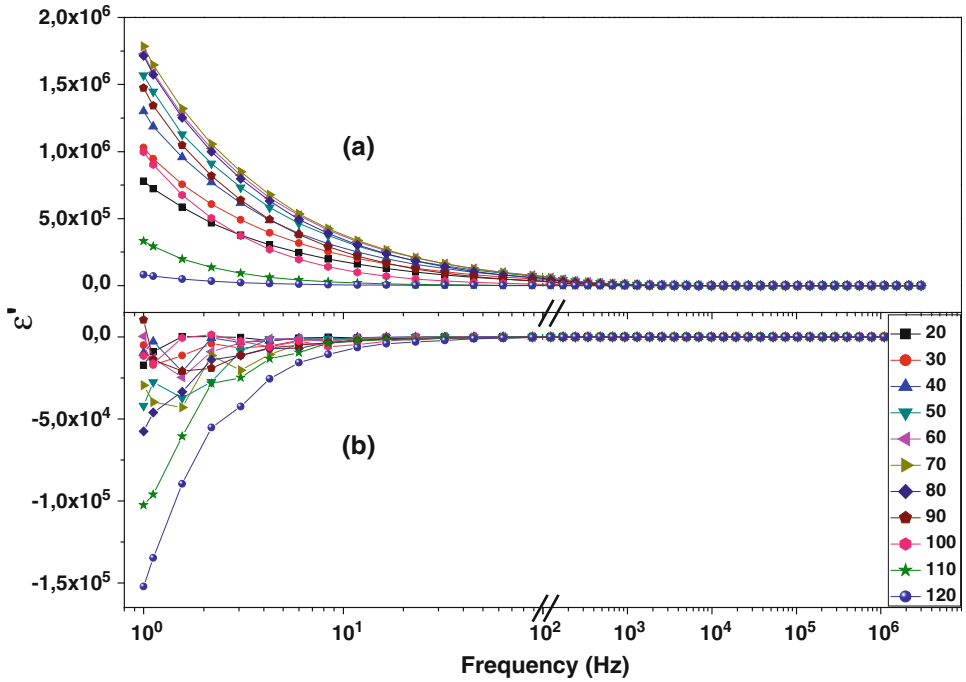

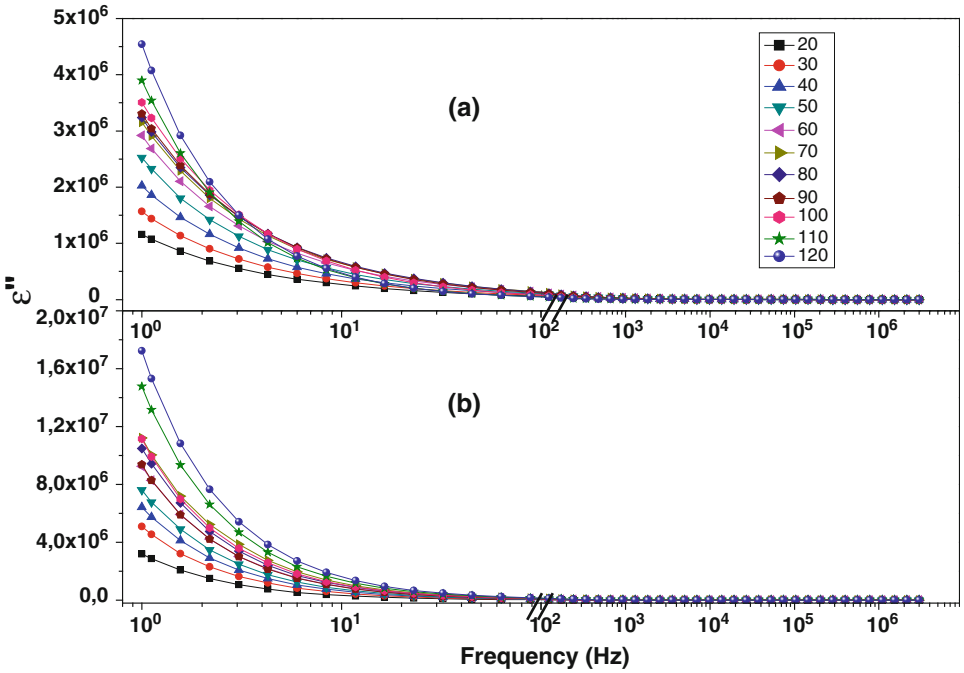

Fig. 10 Frequency dependent imaginary part of permittivity, ε'', as a function of frequency for samples *a* PANI–Fe_3O_4–CTAB and *b* PANI–Fe_3O_4–CTAB–IL at different temperatures

$Ba_{0.8}Rb_{0.4}TiO(C_2O_4)_2$ (BRTCO) nanocomposites [38, 39]. The latter study shows the negative permittivity at frequencies lower than 1 Hz, however, we found PANI composite with negative permittivity high frequency and high temperature. Also the negative permittivity values reach -1.5×10^5. The temperature dependency of changing frequency of negative permittivity is shown in Fig. 9. Also there is a magnetic and PANI composites with negative permittivity in literature [40] but it is just infrared frequency band and the composite is quasi periodic (Fig. 10).

The ε'' of both composites is exponentially decreasing with increasing frequency and increase by increasing temperature. Only at the temperature range of 60–100 °C, the rate of decrease of ε'' (f) curves becomes closer with each other or in different order with temperature increase. The sample with IL has four times larger ε'' values at lower frequencies (nearly 2×10^7) while sample PANI–Fe_3O_4–CTAB has almost ε'' of 5×10^6. This fact is also valid for lower temperature and lower frequency region in which negative permittivity is observed.

4 Conclusion

PANI–Fe_3O_4–CTAB nanocomposite with and without IL are successfully prepared by in situ chemical oxidative polymerization directed with cationic surfactant CTAB. Fabricated materials were characterized by XRD, FTIR, TEM, VSM, and AC–DC electrical conductivity techniques. Crystalline phase has been identified as magnetite, which exhibited nanoparticles with diameters between 5 and 20 nm. Magnetic measurement results show that both PANI–Fe_3O_4–CTAB nanocomposite with and without IL have superparamagnetic properties with M_s of 10.9 and 52 emu g^{-1}, respectively. The IL treatment before cationic CTAB surfactant and PANI polymerization on surface gives drastic decrease in saturation magnetization. Also the mostly seen antiferromagnetic effect at high magnetic fields in MH curves of superparamagnetic systems has not been observed in this IL treated magnetic nanocomposite. Instead just ferromagnetic interactions are noticed. Moreover the IL surface treatment causes important change in dielectric constant of samples. While the PANI–Fe_3O_4–CTAB nanocomposite has positive ε' at elevated temperature and frequencies, the PANI–Fe_3O_4–CTAB–IL nanocomposite has negative ε' values. Generally, the sign change of ε' from "+" to "−" boundary has an exponential increasing function from 30 to 250 Hz with corresponding temperature between 20 and 120 °C. Also the DC conductivity increases about four times by the influence of IL. These magnetic and dielectric findings may lead to new composite materials with uncommon properties in electromagnetic waves scattering and attraction between similar charges. They

potentially can be used as possible high temperature superconductor, negative index materials and microwave absorbers.

Acknowledgments The authors are thankful to the Fatih University, Research Project Foundation (Contract No: P50020902-2) and TUBITAK (Contract No: 110T487) for financial support of this study.

References

1. K.-M. Mangold, J. Schuster, C. Weidlich, Electrochim. Acta **56**, 3616 (2011)
2. M.O. Ansari, F. Mohammad, Sens. Actuators B **157**, 122 (2011)
3. X. Ma, X. Zhang, Y. Li, G. Li, M. Wang, H. Chen, Y. Mi, Macromol. Mater. Eng. **291**, 75–82 (2006)
4. Y. Xie, X. Honga, Y. Gao, M. Li, J. Liua, J. Wanga, J. Lua, Synth. Met. **162**, 677–681 (2012)
5. C. Leng, J. Wei, Z. Liu, J. Shi, J. Alloys Compd. **509**, 3052 (2011)
6. H. Guo, H. Zhu, H. Lin, J. Zhang, Mater. Lett. **62**, 2196 (2008)
7. B. Ünal, Z. Durmus, A. Baykal, H. Sözeri, M.S. Toprak, L. Alpsoy, J. Alloy. Compd. **505**, 172 (2010)
8. H. Erdemi, A. Baykal, E. Karaoglu, M.S. Toprak, Mater. Res. Bull. **47**, 2193 (2012)
9. Z. Durmus, H. Erdemi, A. Aslan, M.S. Toprak, H. Sozeri, A. Baykal, Polyhedron **30**, 419 (2011)
10. S.S. Umarea, B.H. Shambharkara, R.S. Ningthoujam, Synth. Met. **160**, 1815 (2010)
11. J. Jianga, L.H. Ai, D.B. Qina, H. Liu, L.C. Li, Synth. Met. **159**, 695 (2009)
12. T. Wejrzanowski, R. Pielaszek, A. Opalińska, H. Matysiak, W. Lojkowski, K.J. Kurzydlowski, Appl. Surf. Sci. **253**, 204 (2006)
13. R. Pielaszek, Appl. Crystallography Proceedings of the XIX Conference, Krakow, Poland, p 43 (2003)
14. T. Özkaya, M.S. Toprak, A. Baykal, H. Kavas, Y. Köseoğlu, B. Aktaş, J. Alloy. Compd. **472**, 18 (2009)
15. B. Unal, M.S. Toprak, Z. Durmus, H. Sözeri, A. Baykal, J. Nanopart. Res. **12**, 3057 (2010)
16. Z. Durmus, H. Kavas, A. Baykal, H. Sozeri, L. Alpsoy, S.Ü. Çelik, M.S. Toprak, J. Alloy. Compd. **509**, 2555 (2011)
17. M. Aydın, Z. Durmus, H. Kavas, B. Esat, H. Sozeri, A. Baykal, F. Yılmaz, M.S. Toprak, Polyhedron **30**, 1120 (2011)
18. S. Quillard, G. Louarn, S. Lefrant, A.G. MacDiarmid, Phys. Rev. B **50**, 12496 (1994)
19. Z. Durmus, A. Baykal, H. Kavas, H. Sözeri, Physica B **406**, 1114 (2011)
20. H. Guo, H. Zhu, H. Lin, J. Zhang, Mat. Lett. **62**, 2196 (2008)
21. L. Kong, X. Lu, E. Jin, S. Jiang, X. Bian, W. Zhang, C. Wang, J. Solid State Chem. **182**, 2081 (2009)
22. X.F. Lu, Y.H. Yu, L. Chen, H. Mao, W.J. Zhang, Y. Wei, Chem. Commun. **13**, 1522 (2004)
23. Z.J. Wang, J.H. Yuan, M.Y. Li, D.X. Han, Y.J. Zhang, Y.F. Shen, L. Niu, A. Ivaska, J. Electroanal. Chem. **599**, 121 (2007)
24. E.E. Tanrıverdi, A.T. Uzumcu, H. Kavas, A. Demir, A. Baykal, Nano-Micro Lett. **3**, 99 (2011)
25. X. Lu, H. Mao, D. Chao, W. Zhang, Y. Wei, J. Solid State Chem. **179**, 2609 (2006)
26. A. Baykal, M. Günay, M.S. Toprak, H. Sozeri, Effect of ionic liquids on the electrical and magnetic performance of polyaniline-nickel ferrite nanocomposite, Mater. Res. Bull. (2012) (in press)
27. W.J. Liang, M. Bockrath, D. Bozovic, J.H. Hafner, M. Tinkham, H. Park, Nature **411**, 665 (2001)
28. R.H. Kodama, A.E. Berkowitz, E.J. McNiff, S. Foner, Phys. Rev. Lett. **77**, 394 (1996)
29. J.A. Lopez, F. González, F.A. Bonilla, G. Zambrano, M.E. Gómez, Revista Latinoamericana de Metalurgia Materiales **30**, 60 (2010)
30. Z. Durmus, H. Kavas, M.S. Toprak, A. Baykal, T.G. Altınçekiç, A. Aslan, A. Bozkurt, S. Coşgun, J. Alloy. Compd. **484**, 371 (2009)
31. H. Kavas, Z. Durmus, A. Baykal, A. Aslan, A. Bozkurt, M.S. Toprak, J. Non-Cryst. Solids **356**, 484 (2010)
32. B. Unal, Z. Durmus, H. Kavas, A. Baykal, M.S. Toprak, Mater. Chem. Phys. **123**, 184 (2010)
33. E. Temizel, E. Ayan, M. Senel, H. Erdemi, M.S. Yavuz, H. Kavas, A. Baykal, R. Öztürk, Mater. Chem. Phys. **131**, 284 (2011)
34. C.H. Hsieh, A.H. Lee, C.D. Liu, J.L. Han, K.H. Hsieh, S.N. Lee, AIP Adv. **2**, 012127 (2012)
35. J. Joo, E.J. Oh, G. Min, A.G. MacDiarmid, A.J. Epstein, Synth. Met. **69**, 251 (1995)
36. Y.Z. Wang, J. Joo, C.-H. Hsu, A.J. Epstein, Synth. Met. **69**, 267 (1995)
37. V.N. Prigodin, A.J. Epstein, Synth. Met. **125**, 43 (2002)
38. C.W. Chu, F. Chen, J. Shulman, S. Tsui, Y.Y. Xue, W. Wen, P. Sheng, in *SPIE Proceeding*, vol. 5932, ed. by I. Bozovic, D. Pavuna (Optics & Photonics, San Diego, 2005), p. 31
39. C.W. Chu, F. Chen, Y.Y. Xue, J. Shulman, S. Tsui, U.S. Patent 7,611,969 B2, 03 Nov 2009
40. H. Liu, X. Zhao, Chemical route fabricated magnetic structure exhibiting a negative permeability at infrared frequencies. MRS Proc. **919**, (2006). doi:10.1557/PROC-0919-J02-08